Thermally Reversible Surface Morphology Transition in Thin Diblock Copolymer Films

Xiaohua Zhang,* Kevin G. Yager,† Nathaniel J. Fredin, Hyun Wook Ro, Ronald L. Jones, Alamgir Karim,‡ and Jack F. Douglas*

Polymers Division, National Institute of Standards and Technology, Gaithersburg, Maryland 20899. †Current address: Center for Functional Nanomaterials, Brookhaven National Laboratory, Upton, New York 11973. ‡Current address: Department of Polymer Engineering, University of Akron, Akron, Ohio 44325.

ABSTRACT Many phase transitions exhibit ordering transitions at the boundary of the material that are distinct from its interior where intermolecular interactions can be significantly different. The present work considers the existence of a surface thermodynamic order—order transition between two distinct morphologies in thin block copolymer (BCP) films that are of interest in nanomanufacturing applications. Specifically, we find a thermally reversible interfacial transition between sphere-like structures and cylinders in flow-coated films of poly(styrene-*block*-methyl methacrylate) (PS-*b*-PMMA), where the BCP forms a cylinder microphase in the bulk. We present direct evidence from atomic force microscopy (AFM) of ion-etched films and grazing-incidence small-angle X-ray scattering (GISAXS) on films without etching, which shows that the order—order transition is restricted to the outer layer of the film, while the film interior remains in the cylinder state. Moreover, we find this order—order transition to be insensitive to film thickness over the range investigated (40—170 nm). This morphological transition is of importance in characterizing the thermodynamics and dynamics of thin BCP films used as templates in nanomanufacturing applications.

KEYWORDS: block copolymer · thin film · surface morphology · thermal-reversible · transition

There have been many theoretical, computational, and experimental investigations of block copolymer (BCP) ordering in the bulk,[1] but our understanding of BCP ordering in thin films is much less complete. This situation is unfortunate since BCP films are being explored as template materials for memory storage and other nanotechnology applications[2−7] where the control of surface morphology is critical. It is well-known that there can be substantial shifts of the order−disorder transition in thin BCP films.[8] In most experimental studies, researchers essentially have *no idea* where the BCP ordering transitions are and how they become modified by the presence of interacting boundaries. Experimental determination of the ordering transitions in these films has proven difficult, and routine methods of estimating the transition temperature in the bulk, such as rheological measurement,[9] are not readily performed on thin films. Moreover, the study of ordering processes in thin films is often complicated by distinct ordering processes that can occur at the interface of the material. The ordering transition of BCP materials is weakly first-order in nature and can be considered as a kind of mesoscale crystallization process, given that the ordered structures exhibit crystallographic symmetries. These simple observations lead us to expect the existence of distinct thermodynamic transitions occurring at the polymer−air interface, that is, the BCP analogue of surface melting in the crystallization of ordinary small molecular substances. The complex nature of BCP ordering in the bulk also leads to the possibility that distinct order−order transitions, and indeed separate interfacial phase diagrams, may be required to characterize surface ordering in BCP materials. Indeed, the existence of surface transitions is established in liquid crystalline[10−12] and magnetic materials.[13,14] We note that distinct surface order−disorder transitions are also predicted for isolated nanoparticles,[15] so that having multiple ordering transitions is a rather general phenomenon.[16] If such transitions occur in thin BCP films, they would certainly be relevant to applications where these films are used in the ordered state as templates in manufacturing. We investigate the existence of this type of surface transition in model BCP films that have practical interest from a nanomanufacturing standpoint. In particular, we choose an asymmetric BCP that forms cylinders in the bulk, and we investigate the dependence of the surface morphology over a wide temperature range to probe for the existence of reversible thermodynamic transitions at the polymer−air interface. We indeed find a reversible transition between cylinders and

*Address correspondence to xiaohua.zhang@nist.gov, jack.douglas@nist.gov.

Received for review November 19, 2009 and accepted June 07, 2010.

Published online June 16, 2010.
10.1021/nn9016586

This article not subject to U.S. Copyright. Published 2010 by the American Chemical Society.

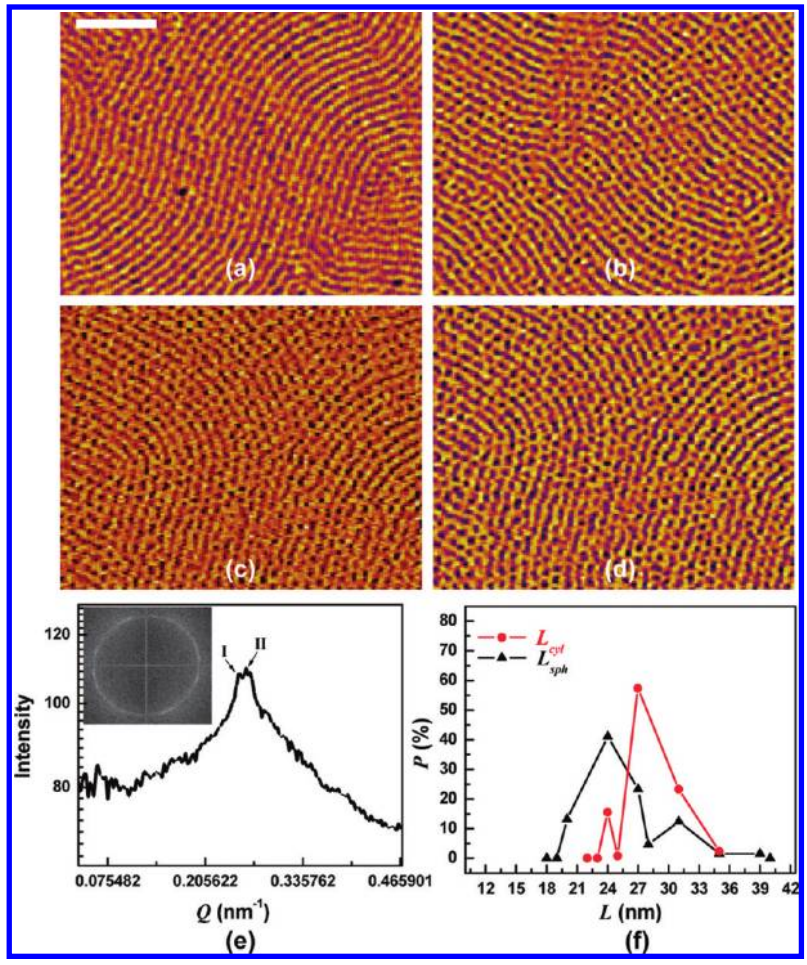

Figure 1. AFM phase images of PS-*b*-PMMA block copolymer films as formed with h_f = 86 nm after annealing for 15 h at 178 °C (a), 180 °C (b), 182 °C (c), and 200 °C (d). The scale bar corresponds to 200 nm and is applied to panels b−d. One-dimensional power spectra by taking a circular average of the intensity of 2D FFT image of panel d is shown in panel e. (f) Probability (*P*) *vs* distances (*L*) measured from the AFM image of PS-*b*-PMMA block copolymer with h_f = 86 nm after annealing at 200 °C for 15 h, where L_{cyl} is constant distance between adjacent parallel rows of the sphere-like structures and L_{sph} is the distance between the sphere-like structures along the axis of the templating cylinder.

sphere-like structures in the surface layer of our BCP film, and we find the transition temperature to be largely insensitive to film thickness.

While a number of previous investigations have observed transitions between a cylinder and sphere morphology in BCP materials, most of these observations have been made on bulk materials. These transitions have usually been induced by changing temperature in the vicinity of an order−disorder phase boundary (defined in terms of the relative compositions of the component polymers and temperature),[17,18] and cylinder−sphere order−order transitions have also been observed by changing relative polymer volume fraction through blending with a homopolymer.[19] Recently, there have been several reports demonstrating an order−order transition between cylindrical and spherical domains under the application of electric fields,[20] shearing,[21] chemical reaction,[7] geometrical confinement in thin films,[22] and other non-equilibrium disturbances. The present work considers a temperature-induced reversible thermodynamic surface transition in thin BCP film where new features are found in comparison to former bulk-oriented studies of BCP ordering.

RESULTS AND DISCUSSION

As described in a previous study,[23] poly(styrene-*block*-methyl methacrylate) (PS-*b*-PMMA) with a total relative molecular mass of 47.7 kg/mol and a mass fraction of PS of 0.74 is used in this study. The diameter and the repeat spacing of cylinders formed in bulk for this block copolymer are 14 and 26 nm, respectively. Our previous results[23] show that, at annealing temperatures below 155 °C, AFM images of the PS-*b*-PMMA sample with the film thickness of 86 nm exhibited cylinders oriented perpendicularly to the polymer interface. The repeat period of the block copolymer is 26 nm, and the number of total layers of the film with the thickness of 86 nm is ≈3.3. In this report, Figure 1 shows the block copolymer morphology of PS-*b*-PMMA that we obtain after allowing the film to order at temperatures above 155 °C. PMMA is the minor component that forms the cylindrical domains in the films. The PMMA component of PS-*b*-PMMA copolymer preferentially segregates to the plasma-treated silicon wafer substrate[1,24] (PMMA favors the silicon oxide substrate because of its lower interfacial energy[25,26]), and correspondingly, we observe the formation of cylinders oriented parallel to the substrate (Figure 1a). The minor phase (PMMA cylinders) and major phase (PS matrix) correspond to darker and lighter regions in the AFM image, respectively. At higher annealing temperatures (Figure 1b−d), however, there is a transition to a different ordered BCP morphology (sphere-like structures) where the cylinder morphology previously existed. The arrangement of the sphere-like structures is distinct from the body-centered cubic (bcc), face-centered cubic (fcc), and hexagonal close-packed (hcp) arrays normally observed in thin films of sphere-forming diblock copolymers. The sphere-like structures seem to be templated laterally in the plane of the film in a manner similar to the underlying parallel cylinders. We have confirmed that this surface order−order transition is independent of film thickness in the range of 40−170 nm (S1 in Supporting Information) and further found that the morphology transition in the temperature range between 178 and 180 °C is insensitive to film thickness (S2 in Supporting Information).

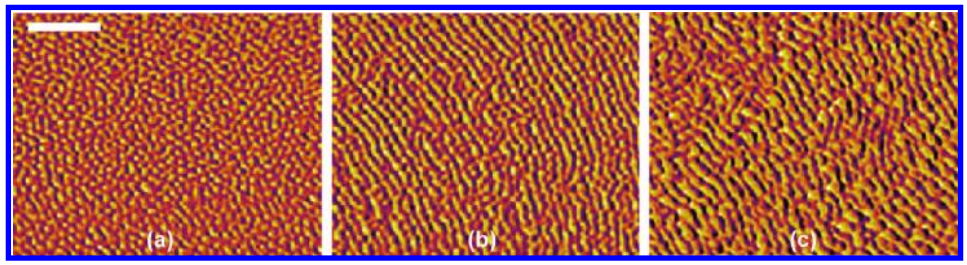

Figure 2. AFM phase images of PS-*b*-PMMA block copolymer films with h_f = 86 nm and annealed at 200 °C for 15 h after etching away ≈10 nm into the film (a) and etching ≈20 nm into the film (b). (c) AFM image after etching ≈20 nm into the film with h_f = 86 nm and annealed at 164 °C for 15 h. The scale bar corresponds to 200 nm and is applied to panels b and c.

The sphere-like morphology is well-established in BCP film after annealing the film for only 8 h (Figure S1 in Supporting Information). To check for a further evolution of structure at later times, we examined these films after 15, 16, 20, and 36 h. No significant evolution of the sphere-like morphology was observed for these films over this extended range of times. These patterns are apparently stable. We have previously reported that the BCP film surface morphology can depend on the method of film formation (flow-coated *versus* spun-cast films), an effect attributed to the trapping of residual solvent (toluene) within the film due to film vitrification while drying.[23] However, we do not expect this residual solvent effect to be important in films ordered at elevated temperatures where the residual solvent should readily be driven off from the film and, indeed, essentially the same sphere-like structures form in both flow-coated and spin-coated BCP film ordering at annealing temperatures above 180 °C (see Figure S3 in Supporting Information). The residual solvent is thus not an issue for this type of surface pattern formation under these high temperature conditions. Next, we characterize the spacings and correlations between the sphere-like structures in Figure 1.

A 2D FFT of Figure 1d, shown as an inset to Figure 1e, indicates a somewhat diffuse ring in reciprocal space describing the sphere-like morphology. The diffuseness of this ring is partially due to the small AFM image size (900 nm × 700 nm) and limited AFM spatial resolution, but there is also a physical factor contributing to this ring diffuseness. In particular, taking a circular average of the intensity of the 2D FFT image reveals that there are two distinct, but close, intensity peaks near 0.23 nm^{-1} (peak I) and 0.26 nm^{-1} (peak II). Correspondingly, the repeat periods evaluated from 1D power spectra FFT intensity peaks are approximately 27 and 24 nm, consistent with a constant distance between adjacent parallel rows of the sphere-like structures (L_{cyl}) and with a distinct distance between the sphere-like structures along the axis of the templating cylinder. Both scales are apparent in the real-space AFM image (Figure 1f). We further explore the morphology of the film and the reversibility of this surface transition below.

In a similar way, we characterize the cylinder morphologies in Figure 2. Figures 2a,b show the AFM phase images after etching away the top 10 and 20 nm of the film, and Figure 2c is the AFM image after etching ≈20 nm into the film containing a surface structure of parallel cylinders with h_f = 86 nm and annealed at 164 °C for 15 h. To quantify the internal structure of the BCP film, we first etch away the uppermost surface layer of the film to expose the internal structure. In principle, the etching technique can provide sequential layer-by-layer images of the sample, so the entire internal film is reconstructed. To achieve an etching process, in which both PS and PMMA are etched at nominally identical rates, we utilized a reactive ion etch (RIE) in O_2 plasma. The film thickness before and after RIE is measured by ultraviolet−visible interferometry with standard uncertainty of ±1 nm. The etching was performed at sufficiently slow rate to facilitate greater depth control, where the etching depth is proportional to the exposure time in the RIE. After etching away the first ≈10 nm of the surface, we observe the sphere-like morphology oriented in a manner similar to parallel cylinders. These observations suggest the sphere-like structures on the surface track the positions of the parallel cylinders. To image the underlying structure of the film, the top layer having a sphere-like morphology (a thickness of approximately 20 nm) was removed with RIE to expose the under-layer for AFM imaging. After etching away the top 20 nm of the film, the parallel cylinders can be clearly discerned (see Figure 2b); this morphology is similar to a 20 nm etching of a film containing a surface structure of parallel cylinders (Figure 2c). On the basis of this depth profiling technique, we conclude that these structures reside in a layer with a depth of 10−20 nm from the top surface. The cylindrical structures within the film suggest that the sphere-like structures on the uppermost layer follow the positions of cylindrical domains within the film. It also appears that the cylinders within the film serve as a substrate pattern upon which the surface sphere-like structures organize. The organization of block copolymer morphology at the surface is thus influenced by ordering within the film, but the surface ordering BCP morphology can evidently be distinct from that of the interior of the film.

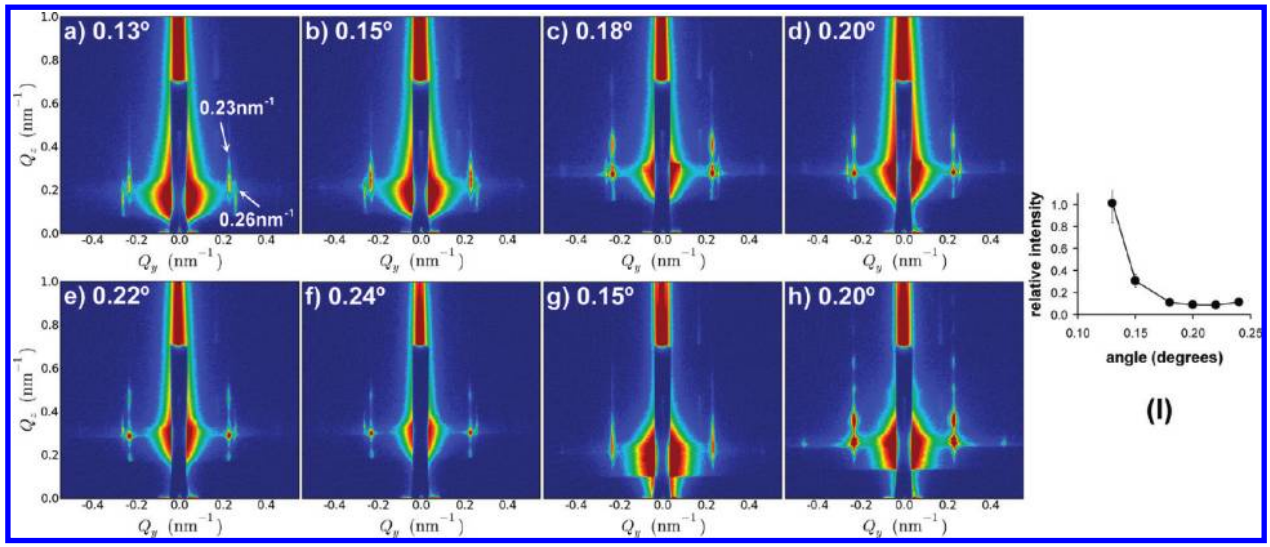

Figure 3. Grazing-incidence small-angle X-ray scattering (GISAXS) detector images for cylinder-forming block copolymer thin films. Q_y and Q_z are defined as coordinates of reciprocal space. The grazing-incidence angles are marked in the panels. (a−f) Film with h_f = 86 nm annealed at 180 °C for 15 h, which exhibits a new surface morphology by AFM. The intensity ratio of peaks at Q_y = 0.26 nm^{-1} and Q_y = 0.23 nm^{-1} at different grazing-incidence angles is shown in panel I. The corresponding *d* spacings at 0.26 and 0.23 nm^{-1} are 24 and 27 nm, respectively. (g,h) Thin film with conventional parallel cylinder morphology for comparison purposes. The weak peaks at Q_y = 0.26 nm^{-1} in panels a−f demonstrate the formation of a distinct surface morphology.

AFM is a 2D characterization method of local surface structure, while GISAXS under favorable circumstances provides 3D information about the film structure. The footprint of GISAXS is 10 mm × 100 μm, and the penetration depth of the X-ray beam depends on the incident angle. GISAXS has much higher resolution compared with AFM and potentially provides much more information about the interior structure of films with periodic ordering. Figure 3 shows grazing-incidence small-angle X-ray scattering (GISAXS) data for represenative BCP thin films. The GISAXS technique involves reflecting a collimated X-ray beam off of the sample and collecting the two-dimensional scattering pattern. This technique is sensitive both to in-plane order and structuring in the film normal direction. Additionally, the technique provides a limited amount of depth control *via* the grazing-incidence angle. For incidence angles below the polymer-vacuum critical angle (which for these films was measured to be θ_c = 0.19°), the X-ray penetration depth for these films is 10 nm and the X-ray beam reflects off of the top of the film. In other words, the measurement is surface-sensitive. For grazing-incidence angles above the polymer-vacuum critical angle, the X-ray penetration depth for these films is above 100 nm and X-ray beam reflects off of the polymer−silicon interface (up to the silicon critical angle of 0.24°) and thus GISAXS probes the entire thin film. By comparing the below and above critical angle data, we can differentiate bulk and surface structures. Careful inspection of the location of the peaks shows that the peak at Q_y = 0.26 nm^{-1} shifts in the vertical direction as the angle changes. When the incoming X-ray beam strikes the sample surface, many of the peaks are from scattering of the reflected beam. Changing incident angle changes the Q_z position of the specular reflection and therefore causes corresponding shifts in peaks due to scattering of that reflection. This probably explains the shift of the peak in vertical direction as the incident angle changes. The scattering patterns in Figure 3 are dominated by a series of intense peaks at Q_y = 0.23 nm^{-1}. Above the critical angle, these scattering peaks can be ascribed to the conventional hexagonally packed cylinders that are aligned parallel to the substrate. Interestingly, the samples which have a unique surface morphology by AFM (Figures 1 and 2) produce an additional peak at Q_y = 0.26 nm^{-1} (Figure 3a−f), which is absent in samples that do not show the surface sphere-like morphology (Figures 3g,h show data for a similar film that is formed of purely parallel-oriented cylinders). This weak scattering peak at Q_y = 0.26 nm^{-1} corresponds to a repeat spacing of ≈24 nm, which matches the spacing seen in the surface structures by AFM. Below the critical angle (surface-sensitive regime), we still see a peak at Q_y = 0.23 nm^{-1}. In this case, the peak arises from the projected cylinder−cylinder distance, which templates the

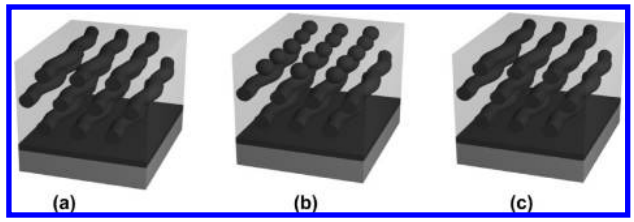

Figure 4. Schematic representation of the self-assembly in PS-*b*-PMMA block copolymer films with thickness of 86 nm at (a) low annealing temperature, (b) high annealing temperature, and (c) high temperature followed by a low annealing temperature. The interfacial "spherical" domains in panel b are an idealization, and the real structure is probably more like the cap-like structures found in micelles supported on surfaces.[27]

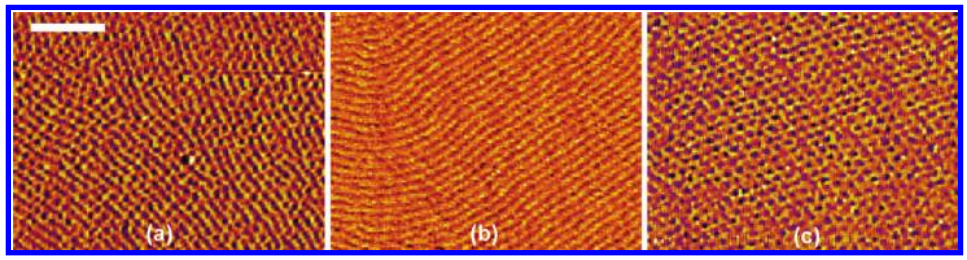

Figure 5. AFM phase images of PS-*b*-PMMA block copolymer films as formed with h_f = 86 nm annealed at 200 °C for 15 h (a) and then further annealed at 164 °C for 24 h (b). (c) Sample shown in panel b is annealed at 200 °C again for 104 h. The scale bar corresponds to 200 nm and is applied to panels b and c.

sphere-like structures. The presence of the $Q_y = 0.26$ nm^{-1} peak when measuring below the critical angle (Figure 3a,b) demonstrates that this distinct morphology exists at the film surface (determined to be sphere-like structure under these conditions in our discussion above). The fact that the strength of this scattering peak, relative to the peak at $Q_y = 0.23$ nm^{-1}, decreases (Figure 3l) as we probe deeper into the film (higher grazing angle) supports our interpretation that this is a purely surface feature. The absence of any *z*-direction structure associated with this higher *Q* peak also implies that it is a thin layer without *z*-direction structure, although it is also possible that the scattering intensity is too low to observe any higher-order peaks in the *z*-direction. The films have an obvious sphere-like surface morphology by AFM, but GISAXS reveals that a large parallel cylinder population exists in the films. In other words, a significant portion of the film must be composed of cylinders laying parallel to the substrate, whereas the top surface evidently exhibits a different morphology. The presence of the $Q_y = 0.26$ nm^{-1} peak below the critical angle is consistent with the AFM observation that the sphere-like structure positions are templated by an underlying cylinder layer, confirming the etching analysis. These structures viewed from the top by AFM have a roughly circular shape, and it is difficult to reconstruct the full three-dimensional structure of these features by AFM alone. However, combination of AFM and GISAXS observations do provide some important information of this BCP interfacial layer. Although we refer to these features on the BCP surface as "spherical" structures, we expect that these structures have a shape more like spherical micelles supported on a surface,[27] where a cap-like structure would be a more appropriate description for the three-dimensional morphology of these interfacial features. The average in-plane radius of the "spheres" obtained from the AFM image is about 6 nm, and the repeat spacing of the sphere-like structures from GISAXS and FFT analyses of the AFM image is 24 nm. The height fluctuations of the film are relatively small in comparison. In particular, the range for the height fluctuation is about 1.5 nm, so that the surface features are relatively flat. The topography we see in sphere-like morphology is then reasonably similar to previous observation on the surface-supported micelles.[27]

What factors control the surface morphology transition? The surface tension of polymers varies with temperature and molecular weight.[28] The polymer−air interface is only weakly selective for PS, which can be expected to make the boundary more susceptible to changes in temperature that alter the balance of polymer-selective interactions. At higher temperatures, the difference in values of surface tension between PS and PMMA blocks becomes smaller,[28] leading to a reduction of the thermodynamic driving force for one block to wet the free surface. Thus, the surface acts as a nonpreferential layer for both blocks.[29,30] This causes a tendency of the considerable rearrangements of microdomains near the surface, a situation that apparently results in the sphere-like structures that we see in Figure 1c,d. Due to a relatively strong affinity for PMMA to substrate, only the uppermost layer can be reconstructed to form this new morphology. Sphere-like structures on the uppermost layer evidently follow the positions of cylindrical domains within the film. It appears that the cylinders within the film serve as a substrate pattern upon which the surface sphere-like structures organize, as illustrated in Figure 4.

We next consider whether this surface morphology transition is an equilibrium phenomenon relating to a surface ordering transition or whether we are observing a purely non-equilibrium phenomenon. To make this check, we test the reversibility of this morphology transition upon varying temperature. If this is an equilibrium transition, then the cylinder morphology should be recovered upon annealing the film with the sphere-like interfacial morphology at a lower temperature. Figure 5b shows an AFM phase image of a PS-*b*-PMMA block copolymer film annealed at 200 °C for 15 h and then annealed at 164 °C for 24 h. Sphere-like microdomains having a string-like alignment are formed as before at the higher temperature (Figure 1d), while the cylinder morphology is recovered upon cooling, as illustrated in Figure 4. This transition involves only local rearrangements of the block copolymer molecules rather than large length-scale rearrangements of microdomains, which presumably makes the transition more facile than other BCP thin film transitions. We also address the important matter of reversibility of the BCP surface morphology. This process can indeed be sluggish kinetically, and long annealing times can be re-

quired to fully observe the full reconversion to sphere-like structures. Figure 5c shows an AFM phase image of the regenerated surface morphology found after annealing at 200 °C for 104 h. After this long period, the film has substantially converted to the sphere morphology. The conversion to the sphere-like morphology was much more limited after 60 h (image not shown). The reconversion to the sphere morphology is clearly kinetically sluggish.

CONCLUSIONS

We investigate a thermoreversible order−order transition between sphere-like structures and cylinders on the top surface of thin PS-*b*-PMMA diblock copolymer thin films using atomic force microscopy, etching, and GISAXS. Our results indicate that the morphology of block copolymer films depends not only on the relative volume fraction of constituent polymers of the block copolymer and temperature as in the bulk but also on a temperature-dependent surface energy. Varying the temperature changes the balance of the selective polymer surface interactions, and this variation is apparently sufficient to induce a morphology transition at the surface of the film. Both AFM and GISAXS measurements indicate that the positions of the sphere-like structures appear to correlate with a cylindrical morphology in the film, so that the packing normally observed in thin films of sphere-forming diblock copolymers is not possible in these surface morphologies. Potential practical applications, for example, patterned magnetic recording media, require nanostructures aligned in rows, and the transition we discuss would compromise the BCP materials as an effective template for this application. A technique, called "molecular transfer printing" (MTP)[31] takes advantage of patterns in the domain structure at the surface of block copolymer films and transfers those patterns with high fidelity to substrates placed in contact with the copolymer film. By MTP, the surface pattern from one BCP film can be transferred to a second substrate to form a chemical template for a new BCP. Our research indicates that at high temperature a layer of sphere-like microdomains was formed above parallel cylinder layer and aligned with the underneath cylinders oriented parallel to substrate. This new type of BCP order−order transition may be useful for fabricating arrays of spots or holes assembled in rows by transferring patterns into an underlying layer of silica if the cylinder orientation below in the film is controlled by ordering in channels or chemically patterned surfaces. Moreover, this phenomenon is certainly relevant to the general engineering problem of controlling the surface morphology.

From a more fundamental perspective, the existence of this type of surface morphology transition means that there is need for greater effort in determining not only the phase diagram governing the order−disorder transition of thin block copolymer films, but we must also consider distinct order−disorder transition curves governing the boundaries of the films.

EXPERIMENTAL DETAILS

Preparation of BCP Thin Films. PS-*b*-PMMA with a total relative molecular mass of 47.7 kg/mol and a mass fraction of PS of 0.74 was purchased from Polymer Source, Inc.[32] PS-*b*-PMMA films were prepared *via* flow coating[33] from a 4% by mass block copolymer solution in toluene onto plasma-treated Si wafers. The film thickness was characterized with ultraviolet−visible interferometry (0.5 mm diameter with standard uncertainty of ±1 at 500 nm film thickness[34]). The samples were placed in a vacuum oven to anneal at different *T*. A typical procedure for generating a block copolymer film *via* flow coating is outlined as follows. The substrate is affixed to the translation stage. A knife blade is mounted on the tip-tilt-rotation stage. The blade is positioned at a fixed angle of 5° in our system and brought down into contact with the substrate. At this point, the blade tilt is adjusted to bring the blade level with the surface of the substrate. The blade is then elevated to a given height above the substrate (typically 200 μm), and a bead of polymer solution (typically 50 μL for a 25 mm wide blade) is syringed along the leading edge of the blade. Since the blade height is only a couple hundred micrometers, capillary forces wick and hold the solution under the blade. Once the solution is placed under the knife blade, the operational commands are sent to the translation stage to initiate the desired motion. As the stage moves, a liquid film remains behind. The liquid film then dries to a solid film whose thickness is determined by the solids concentration in the wet film.

Atomic Force Microscope. AFM images were obtained in phase mode with an Asylum MFP-3D scanning force microscope in the tapping mode. The tapping mode cantilevers with spring constant ≈50 N/m, resonance frequency range from 100 to 200 kHz, and the drive frequency with the offset of −5% were used. The minor phase (PMMA cylinders) and major phase (PS matrix) correspond to darker and lighter regions in the AFM image, respectively. Multiple 2 μm × 2 μm AFM images were collected for each annealing condition so as to obtain proper sampling statistics.

Reactive Ion Etching (RIE). Removal of the top surface of block copolymer thin films was done by using a Unaxis 790 plasma RIE tool with oxygen source. RIE is a plasma-based process that uses radio frequency (RF) power to drive the chemical reaction. RIE is a process of physical etching combined with a chemical reaction. In RIE, the substrate is placed inside a reactor in which several gases are introduced. A plasma is formed in the gas mixture using an RF power source that ionizes the gas molecules. The ions are accelerated toward and react at the surface of the material being etched, forming another gaseous material. There is also a physical interaction aspect to the etching. If the ions have high enough energy, they can knock atoms out of the material to be etched without a chemical reaction. The dry etch process involves a complex balance of chemical and physical etching and depends on many parameters. Since the ions react with materials on the sample surface, the molecular weights on the sample surface change during RIE. For BCP films, the ion-assisted etching is the dominant mechanism for O_2 RIE and has a minimal effect on the pattern fidelity.[35] Therefore, the pure oxygen plasma was chosen to preserve the initial morphology of the BCP film. A RIE recipe (O_2 flow of 10 sccm, pressure of 50 mTorr, power of 50 W, and a temperature of 25 °C) was selected after measuring the etching rate for the blanket films. A slightly higher etching rate is observed for PMMA, but the difference is minimal for the short time RIE used in this study. Both PS and PMMA are etched at nominally identical rates (approximately 1.0 nm/s determined by X-ray reflectivity and white light reflectometer), and thus the

volume fraction of PS and PMMA in the BCP film remains almost constant. The samples with target etching thickness of 10 and 20 nm were prepared by applying 10 and 20 s etching times.

Grazing-Incidence Small-Angle X-ray Scattering (GISAXS). Measurements were performed at Argonne's Advanced Photon Source using the 8-ID-E beamline. Two-dimensional scattering images were measured using a charge-coupled device (CCD) detector at a distance of 1.975 m and an X-ray wavelength of 0.169 nm (photon energy of 7.35 keV). Samples were measured under vacuum at incident angles both above and below the polymer-vacuum critical angle, which was determined using an X-ray reflectivity scan to be $\theta_c = 0.19°$.

Acknowledgment. This work was funded in part by the National Institute of Standards and Technology (NIST) Office of Microelectronics Programs. K.G.Y. acknowledges the support of Natural Sciences and Engineering Research Council (NSERC) of Canada in the form of a Postdoctoral Fellowship. N.J.F. acknowledges the support of the National Research Council (NRC)-NIST Postdoctoral Fellowship Program. We also wish to thank Joseph Strzalka for help with X-ray scattering measurements. Use of the Advanced Photon Source was supported by the U.S. Department of Energy, Office of Science, Office of Basic Energy Science, under Contract No. W-31-109-Eng-38.

Supporting Information Available: AFM images of BCP thin films with the film thickness in the range of 40−170 nm and annealed at different temperatures for film thickness of 104 nm. This material is available free of charge *via* the Internet at http://pubs.acs.org.

REFERENCES AND NOTES

1. Bates, F. S.; Fredrickson, G. H. Block Copolymer Thermodynamics: Theory and Experiment. *Annu. Rev. Phys. Chem.* **1990**, *41*, 525–557.
2. Segalman, R. A. Patterning with Block Copolymer Thin Films. *Mater. Sci. Eng., R* **2005**, *48*, 191–226.
3. Segalman, R. A.; Hexemer, A.; Hayward, R. C.; Kramer, E. J. Ordering and Melting of Block Copolymer Spherical Domains in 2 and 3 Dimensions. *Macromolecules* **2003**, *36*, 3272–3288.
4. Krausch, G. Surface-Induced Self Assembly in Thin Polymer Films. *Mater. Sci. Eng., R* **1995**, *14*, 1–94.
5. Park, C.; Yoon, J.; Thomas, E. L. Enabling Nanotechnology with Self Assembled Block Copolymer Patterns. *Polymer* **2003**, *44*, 6725–6760.
6. Cheng, J. Y.; Ross, C. A.; Smith, H. I.; Thomas, E. L. Templated Self Assembly of Block Copolymers: Top-Down Helps Bottom-Up. *Adv. Mater.* **2006**, *18*, 2505–2521.
7. La, Y. H.; Edwards, E. W.; Park, S. M.; Nealey, P. F. Directed Assembly of Cylinder-Forming Block Copolymer Films and Thermochemically Induced Cylinder to Sphere Transition: A Hierarchical Route to Linear Arrays of Nanodots. *Nano Lett.* **2005**, *5*, 1379–1384.
8. Shin, C.; Ahn, H.; Kim, E.; Ryu, D. Y.; Huh, J.; Kim, K.-W.; Russell, T. P. Transition Behavior of Block Copolymer Thin Films on Preferential Surfaces. *Macromolecules* **2008**, *41*, 9140–9145.
9. Wunderlich, B. Thermodynamics and Kinetics of Crystallization of Flexible Molecules. *J. Polym. Sci., Part B: Polym. Phys.* **2008**, *46*, 2647–2659.
10. Ocko, B. M.; Braslau, A.; Pershan, P. S.; Als-Nielsen, J.; Deutsch, M. Quantized Layer Growth at Liquid-Crystal Surfaces. *Phys. Rev. Lett.* **1986**, *57*, 94–97.
11. Ocko, B. Smectic-Layer Growth at Solid Interfaces. *Phys. Rev. Lett.* **1990**, *64*, 2160–2163.
12. Li, H.; Paczuski, M.; Kardar, M.; Huang, K. Surface Ordering and Finite-Size Effects in Liquid-Crystal Films. *Phys. Rev. B* **1991**, *44*, 8274–8283.
13. Binder, K. *Phase Transitions and Critical Phenomena*; Academic Press: London, 1983.
14. Nakanishi, H.; Fisher, M. Multicriticality of Wetting, Prewetting, and Surface Transitions. *Phys. Rev. Lett.* **1982**, *49*, 1565–1568.
15. Cheng, H.-P.; Berry, R. S. Surface Melting of Clusters and Implications for Bulk Matter. *Phys. Rev. A* **1992**, *45*, 7969–7980.
16. Ocko, B. M.; Wu, X. Z.; Sirota, E. B.; Sinha, S. K.; Gang, O.; Deutsch, M. Surface Freezing in Chain Molecules: Normal Alkanes. *Phys. Rev. E* **1997**, *55*, 3164–3182.
17. Kimishima, K.; Koga, T.; Hashimoto, T. Order−Order Phase Transition between Spherical and Cylindrical Microdomain Structures of Block Copolymer. I. Mechanism of the Transition. *Macromolecules* **2000**, *33*, 968–977.
18. Sakurai, S.; Hashimoto, T.; Fetters, L. J. Thermoreversible Cylinder−Sphere Transition of Polystyrene-*block*-Polyisoprene Diblock Copolymers in Dioctyl Phthalate Solutions. *Macromolecules* **1996**, *29*, 740–747.
19. Vaidya, N. Y.; Han, C. D.; Kim, D.; Sakamoto, N.; Hashimoto, T. Microdomain Structures and Phase Transitions in Binary Blends Consisting of a Highly Asymmetric Block Copolymer and a Homopolymer. *Macromolecules* **2001**, *34*, 222–234.
20. Tsori, Y.; Tournilhac, F.; Andelman, D.; Leibler, L. Structural Changes in Block Copolymers: Coupling of Electric Field and Mobile Ions. *Phys. Rev. Lett.* **2003**, *90*, 145504-1–145504-4.
21. Hong, Y.-R.; Adamson, D. H.; Chaikin, P. M.; Register, R. A. Shear-Induced Sphere-to-Cylinder Transition in Diblock Copolymer Thin Films. *Soft Matter* **2009**, *5*, 1687–1691.
22. Niihara, K.-I.; Sugimori, H.; Matsuwaki, U.; Hirato, F.; Morita, H.; Doi, M.; Masunaga, H.; Sasaki, S.; Jinnai, H. A Transition from Cylindrical to Spherical Morphology in Diblock Copolymer Thin Films. *Macromolecules* **2008**, *41*, 9318–9325.
23. Zhang, X.; Berry, B. C; Yager, K. G.; Kim, S.; Jones, R. L.; Satija, S.; Pickel, D. L; Douglas, J. F.; Karim, A. Surface Morphology Diagram for Cylinder-Forming Block Copolymer Thin Films. *ACS Nano* **2008**, *2*, 2331–2341.
24. Coulon, G.; Russell, T. P.; Green, P. F.; Deline, V. R. Surface-Induced Orientation of Symmetric, Diblock Copolymers: A Secondary Ion Mass-Spectrometry Study. *Macromolecules* **1989**, *22*, 2581–2589.
25. Huang, E.; Pruzinsky, S.; Russell, T. P.; Mays, J.; Hawker, C. J. Neutrality Conditions for Block Copolymer Systems on Random Copolymer Brush Surfaces. *Macromolecules* **1999**, *32*, 5299–5303.
26. Morkved, T. L.; Lopes, W. A.; Hahm, J.; Sibener, S. J.; Jaeger, H. M. Silicon Nitride Membrane Substrates for the Investigation of Local Structure in Polymer Thin Films. *Polymer* **1998**, *39*, 3871–3875.
27. Krishnamoorthy, S.; Pugin, R.; Brugger, J.; Heinzelmann, H.; Hinderling, C. Tuning the Dimensions and Periodicities of Nanostructures Starting from the Same Polystyrene-block-Poly(2-vinylpyridine) Diblock Copolymer. *Adv. Funct. Mater.* **2006**, *16*, 1469–1475.
28. Wu, S. Surface and Interfacial Tensions of Polymers, Oligomers, Plasticizers, and Organic Pigments. In *Polymer Handbook*; Brandrup, J., Immergut, E. H., Grulke, E. A., Eds.; John Wiley and Sons: New York, 1999; pp VI/521−VI/541.
29. Wang, Q.; Nealey, P. F.; de Pablo, J. J. Monte Carlo Simulations of Asymmetric Diblock Copolymer Thin Films Confined Between Two Homogeneous Surfaces. *Macromolecules* **2001**, *34*, 3458–3470.
30. Dong, M.; Qiang, W. Hard-Surface Effects in Polymer Self-Consistent Field Calculations. *J. Chem. Phys.* **2007**, *126*, 2349021-1–2349021-10.
31. Ji, S.; Liu, C.-C.; Liu, G.; Nealey, P. F. Molecular Transfer Printing Using Block Copolymers. *ACS Nano* **2010**, *4*, 599–609.
32. Certain equipment, instruments, or materials are identified in this paper in order to adequately specify the experimental details. Such identification does not imply recommendation by the NIST, nor does it imply the materials are necessarily the best available for the purpose.
33. Stafford, C. M.; Roskov, K. E.; Epps, T. H.; Fasolka, M. J.

Generating Thickness Gradients of Thin Polymer Films *via* Flow Coating. *Rev. Sci. Instrum.* **2006**, *77*, 023908-1–023908-7.
34. The data in this article and in the figures are presented along with the standard uncertainty involved in the measurement, where the uncertainty represents one standard deviation from the mean.
35. Liu, C.; Nealey, P. F.; Ting, Y.; Wendt, A. E. Pattern Transfer Using Poly(styrene-block-Methyl methacrylate) Copolymer Films and Reactive Ion Etching. *J. Vac. Sci. Technol., B* **2007**, *25*, 1963–1968.